PCCP

PAPER

View Article Online
View Journal | View Issue

Cite this: *Phys. Chem. Chem. Phys.*, 2014, **16**, 13477

Defect-induced semiconductor to metal transition in graphene monoxide

Jungwook Woo, Kyung-Han Yun, Sung Beom Cho and Yong-Chae Chung*

Received 8th April 2014,
Accepted 19th May 2014

DOI: 10.1039/c4cp01518e

www.rsc.org/pccp

This study investigates the influence of point defects on the geometric and electronic structure of graphene monoxide (GMO) *via* density functional theory calculations. In aspects of defect formation energy, GMOs with oxygen vacancies and bridge interstitial defects are more likely to form when compared to GMOs with defects such as carbon vacancies and hollow interstitial defects. It was also found that the oxygen vacancy or the hollow interstitial defect induces local tensile strain around the defective site and this strain increases the band gap energy of the defective GMO. In addition, the band gaps of GMO with carbon vacancies or bridge interstitial defects decreased mainly due to the dangling bonds, not due to the strain effect. It is noted that the dangling bond derived from the defects forms the defect-level in the band gap of GMO. The semiconductor to metal transition by the band gap change (0–0.7 eV) implies the possibility for band gap engineering of GMO by vacancies and interstitial defects.

1. Introduction

Since graphene was mechanically exfoliated,[1] the remarkable electronic properties of graphene have become some of the most attractive topics of research.[1–3] Because of its unprecedented electronic properties, a lot of effort has been devoted to the application of graphene in electronics.[4,5] However, the zero-gap of graphene prevents applications in electronics that require a certain band gap. To overcome the semi-metallic properties of graphene, there have been many studies such as bilayer graphene through gating effects,[6] interactions with substrates,[7,8] and the formation of graphene nanoribbons (GNRs),[9,10] graphene quantum dots (GQDs)[11] and chemically modified graphene.[12]

One of the many attempts to generate a band gap of graphene is by chemically modifying graphene, such as graphene monoxide (GMO).[13] Recently, it has been reported that graphene monoxide can be synthesized through the vacuum annealing of the graphene oxide multilayer. The effective mass of carriers in GMO is lighter than that of Si.[14] In addition, in a previous study,[14] the applied strain can control a lattice parameter and this leads to a change in the band gap of GMO. Due to an easily tunable band gap, GMO may broaden the potential applications in electronics, such as sensors, optoelectronic devices and transistors.

Because defects govern various characteristics of technological materials like semiconductors, defects fatally influence the electronic properties of crystals.[15] At the same time, defects can be advantageous in some cases.[16,17] In addition, according to the second law of thermodynamics, there is an inevitable disorder in crystalline materials and several defects may be generated during the synthesis or processing.[18] Particularly, vacancies are the main defects derived from the synthesis of carbon nanostructures such as GMOs.[19] Furthermore, defects can also be deliberately introduced into this material by irradiation or chemical treatments.[20,21] For this reason, it is necessary to investigate how point defects influence GMO, and for application in electronic devices, the change in properties caused by the defects in GMO must also be understood.

In this study, using density functional theory calculations, the possible changes in electronic properties of GMO were investigated referring to formable point defects, such as carbon, oxygen vacancies and interstitial oxygen defects. For this reason, it is necessary to investigate how point defects influence GMO and for application in electronic devices, changes in properties by a defect in GMO must be understood. In this research, the geometric and electronic structure of GMO, where the point defect appears, will be briefly discussed. By point defects, a reconstructed atom arrangement occurs in GMO. This investigation indicates that the point defects can change the properties of GMO, and the potential application in electronic devices. Furthermore, the electronic band structure of defective GMO is calculated to investigate the change in electronic properties by point defects.

2. Computational details

DFT calculations were performed using the Vienna *ab initio* simulation package (VASP) code.[22] The plane-wave basis set was

Department of Materials Science and Engineering, Hanyang University, 17 Haengdang-dong, Seongdong-gu, Seoul 133-791, Republic of Korea. E-mail: yongchae@hanyang.ac.kr; Tel: +82-2-2296-5308

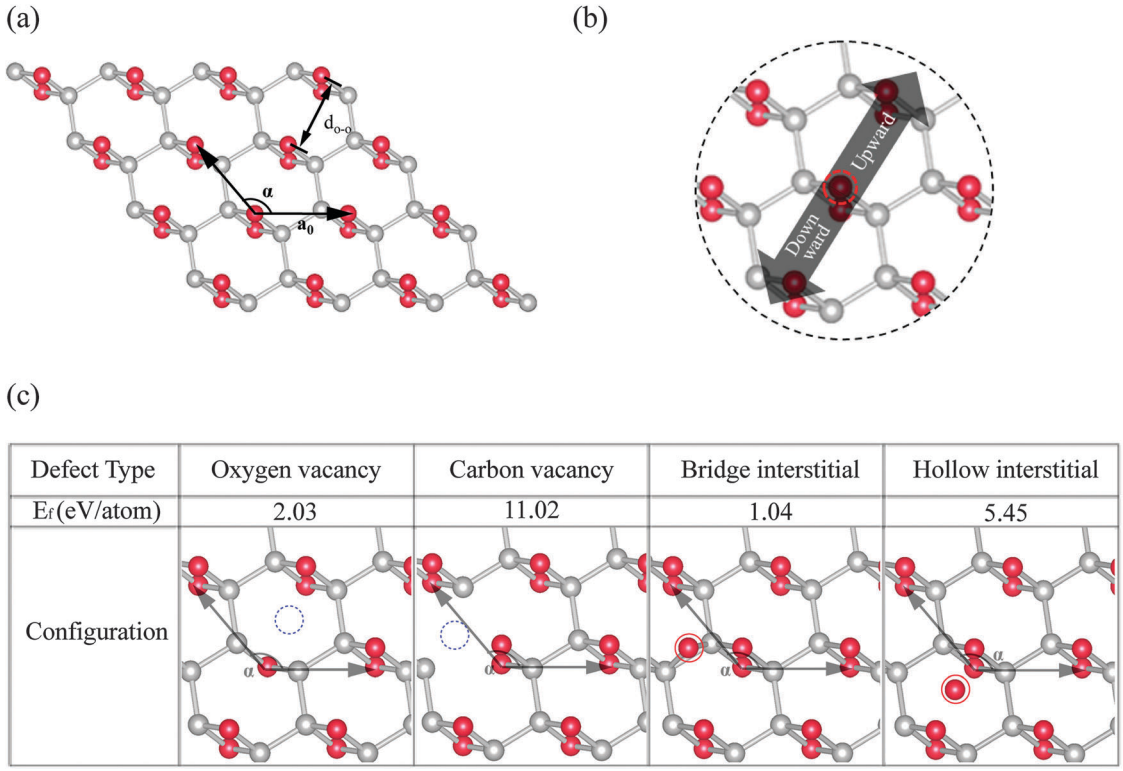

Fig. 1 Schematic view of the point defects of GMO. Carbon and oxygen atoms are colored gray and red, respectively. (a) Structure of GMO and structural parameters of GMO are labeled. (b) Arbitrary directions (upper or lower) from one of neighboring oxygen atoms around the defect in Table 1 are labeled. (c) Configuration of defective GMO and formation energy of defective GMO. Blue dash and a red circle in configuration are the positions of the interstitial defect and the vacancy. Lattice opening angle α of defective GMO is labeled.

expanded to a cut off energy of 500 eV. Projector-augmented waves (PAW)[23] were used to describe the ion cores, and the exchange–correlation interactions were expressed with a generalized gradient approximation (GGA)[24,25] in the form of the Perdew, Burke, and Ernzerhof (PBE) functional.[26] All of the self-consistent loops were iterated until the total energy difference of the systems between the adjacent iterating steps became less than 10^{-5} eV. The calculations were performed with a Gamma-point centered 6 × 6 × 1 *k*-point generated by the Monkhorst–Pack scheme.[27] All the calculations were performed using collinear spin polarization. The simulation model was placed in a 20 Å vacuum spacer to avoid interaction between the two adjacent periodic images. The Hellmann–Feynman force on each atom was less than 0.02 eV $Å^{-1}$.[28] Ionic relaxation was executed using the conjugate gradient method.

The lattice parameters of GMO (a_0 = 3.13 Å, α = 130°) are obtained through the lattice parameter optimization (Fig. 1(a)). For the defect calculation, the GMO was modeled as a 4 × 4 supercell and the defects were induced by removing and adding a single atom through DFT calculations.

3. Results and discussions

The possible point defects and defect formation energies are illustrated in Fig. 1. The carbon and oxygen vacancies and the two interstitial oxygen defects of the bridge and hollow sites exclude the on-top site,[28] because the oxygen located on the on-top site is in close proximity to the oxygen atom of the double-epoxide pair. The defect formation energies (E_f) are calculated for each of the configuration of defective GMO. E_f is defined as:

$$E_f = E_{defect} - E_{perfect} \pm \mu_{atom} \quad (1)$$

where E_{defect} and $E_{perfect}$ are the energies of the defective and perfect GMO, and μ_{atom} is the chemical potential of the isolated atoms (C and $1/2O_2$). The negative sign of the atomic chemical potential (μ_{atom}) is for the case of the oxygen interstitial and the positive sign is for both cases of the oxygen and the carbon vacancy. From an energy point of view, the oxygen vacancy and the interstitial oxygen on the bridge site are more stable to be formed compared to the other two defects, where there is a carbon vacancy and an interstitial oxygen at the hollow site (Fig. 1(c)). Since the epoxy pair is energetically less stable than the carbonyl pairs,[29] the formation of interstitial oxygen on the bridge site needs less formation energy than that of the hollow site. It was also confirmed that the carbon vacancy (the formation energy of 11.02 eV) is hard to form due to the strong covalent bonds of neighboring carbon atoms.

The change in band gap energies for each defect species based on that of perfect GMO indicates how sensitively the electronic properties respond to the local geometric and electronic structure change. In comparison with the band gap of

Table 1 Structural parameters around defects and band gaps of defective GMO. Upward* is the arbitrary direction from most neighboring oxygen atoms near the defect. Downward* is the opposite direction of upward*

		Perfect		Oxygen vacancy		Carbon vacancy		Bridge interstitial		Hollow interstitial	
		d_{O-O} (Å)	α (°)	d_{O-O} (Å)	α (°)	d_{O-O} (Å)	α (°)	d_{O-O} (Å)	α (°)	d_{O-O} (Å)	α (°)
Direction	Upward*	2.64	130.0	2.71	128.5	2.63	129.9	2.59	130.7	2.66	129.6
	Downward*	2.64	130.0	2.75	128.5	2.69	128.8	2.72	127.7	2.61	129.3
Band gap (eV)		0.525		0.727		0.261		0.000		0.633	

perfect GMO (0.525 eV), the band gap of GMO with oxygen vacancies and interstitial oxygen on the hollow site increases to 0.727 eV and 0.633 eV. However, the band gap of carbon vacancies and the interstitial oxygen on the bridge site decreases to 0.261 eV and 0 eV. Interestingly, the interstitial oxygen invading the bridge site changes the semiconducting GMO into a metallic GMO. Previously, Pu *et al.* reported that the band gap of GMO sensitively responds to changes in the opening angle α and increases with a decrease of the opening angle α.[14] In light of the strain effect derived from the change in the opening angle α by defect formation, the local strain field could be generated by defect and affect the electronic properties. The standard definition of the lattice angle is the angle between the lattice vectors in pristine GMO. The defined lattice angle is equal to the angle of the oxygen atoms and the oxygen atoms of the next unit cell (in Fig. 1(a)). However, due to the unclear lattice vector of the defective region, the lattice angle of the defective GMO is defined as the angle between the neighboring oxygen atom near the defect and the oxygen atoms of the next unit cell (in Fig. 1(c)). The lattice opening angle α of the defective GMO decreases overall from the opening angle of the perfect GMO, except for that of defective GMO with interstitial oxygen on the bridge interstitial site (Table 1). The tendency of the band gap energy, according to the defect species, is in good agreement with the previous study of the strain effect on band gap energies of GMO.[14] However, since the strain effect is restricted to the area locally formed by a point defect, the band gap energy of this system does not perfectly coincide with the previous study. The increases of the band gap of GMO with an oxygen vacancy and a hollow interstitial defect show a similar trend to that of the previous study.[14] However, in contrast to the oxygen vacancy and the hollow interstitial defect, the decreases of the band gap of carbon vacancies and bridge interstitial defects are different from the trend of the strain effect of GMO. As shown in Fig. 2, it is noticed that the band gap of the structures with local tensile strain near the defect (oxygen vacancies and hollow interstitial defects) increases from the band gap of the perfect GMO, and the band gap of the structures with local compressive strain near the defect (carbon vacancies and bridge interstitial defects) decreases.

The dangling bonds toward the missing atom to the neighboring atoms are left by the oxygen vacancy. By the Jahn–Teller effect, which leads to saturation of the dangling bonds, two carbon atoms are connected to each other.[18] Unlike the oxygen vacancy, the dangling bonds caused by the carbon vacancy are unsaturated (in Fig. 2(c)). When the interstitial oxygen atom occupies the hollow site, the interstitial oxygen atom pushes oxygen atoms of the double-epoxide pair and it leads to a distorted hexagonal cell of GMO. On the other hand, oxygen adsorption in the bridge site of GMO breaks the double-epoxide pair around the interstitial defect and the interstitial oxygen

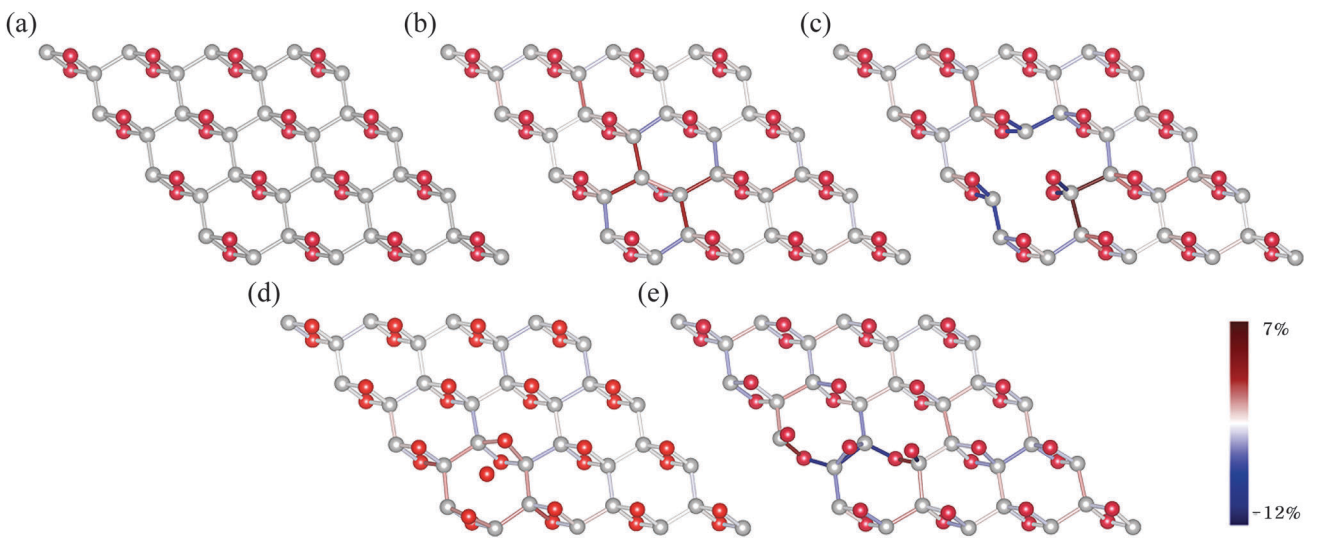

Fig. 2 Relaxed structures of GMO and the strain field near the defect. (a) Perfect GMO, GMO with (b) oxygen vacancy, (c) carbon vacancy, (d) oxygen hollow interstitial defect, (e) oxygen bridge interstitial defect. The atomic bonding lengths are colored according to the increase (red) or decrease (blue) from the bonding length of perfect GMO. The atomic bonds are colored according to the color bar in the variation of the bond length between defective GMO and perfect GMO.

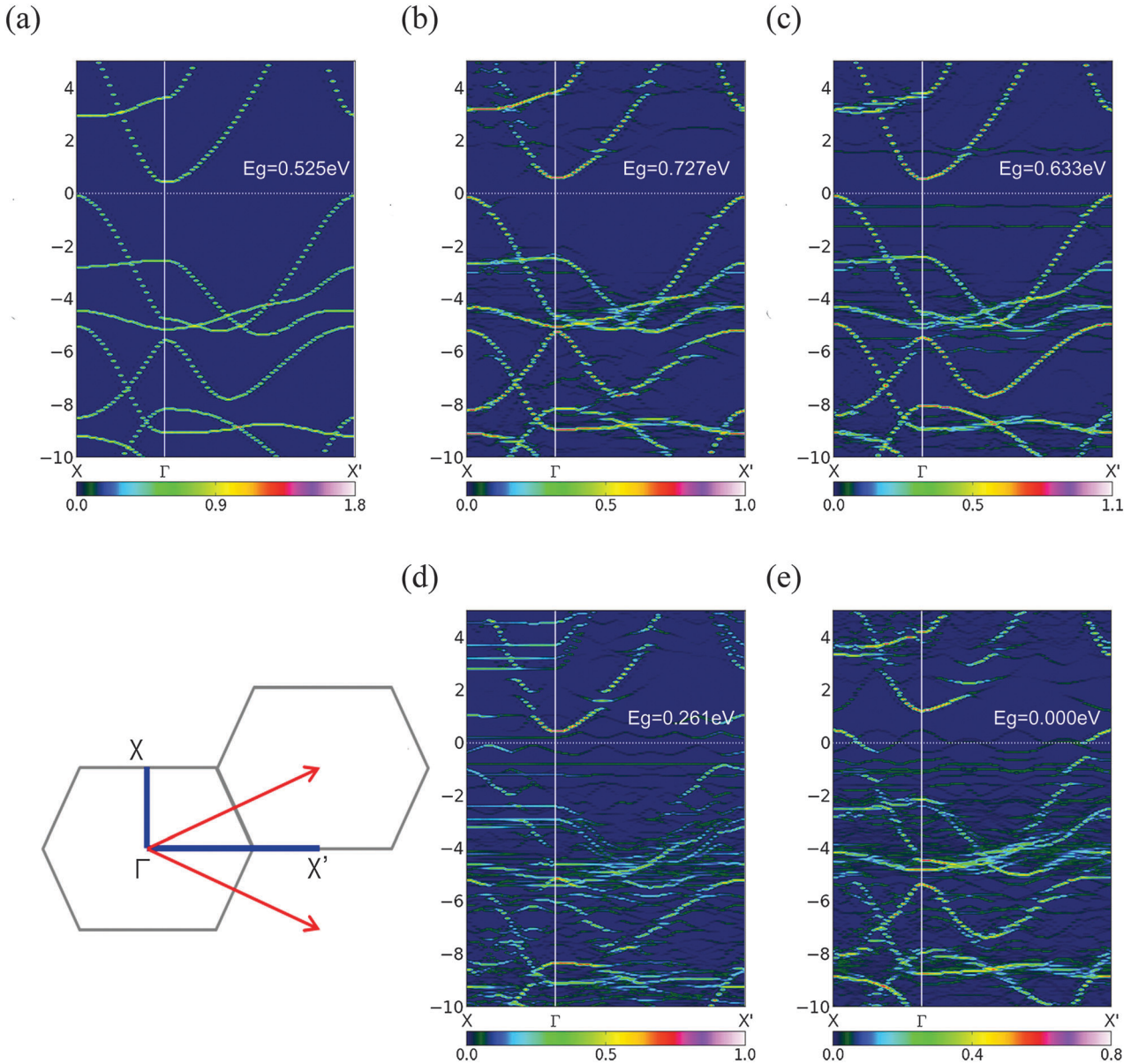

Fig. 3 (unfolded) Band structure of perfect and defective GMO: (a) perfect GMO. GMO with (b) oxygen vacancies, (c) oxygen hollow interstitial defects (d) carbon vacancies, and (e) oxygen bridge interstitial defects. The scale of the color bar below the band structure is the number of primitive cell bands crossing the interval (0.05 eV) at a given primitive wave-vector. The inset figure is the schema of high symmetry points in the Brillouin zone.

interacts with carbon atoms of the bridge site. Breaking the double-epoxide bonds causes the oxygen atom to have a remaining dangling bond and it closes with the carbon atom on the opposite bridge site.

Fig. 3 shows the effective (unfolded)[30] band structures of defective GMO. In the effective band structure, it seems that the overall outline of the band structure remains except for the defect-induced level and the smearing of the primitive cell eigenvalues. In the unfolded band structure of the perfect supercell (in Fig. 3(a)), in principle, the value of the spectral weight (color bar scale) must be integers. However, when using PAW not true Kohn–Sham eigenstates in VASP, the values of the spectral weight deviate slightly from the integers.[31] In the effective band structure[30] of the local tensile strain near the defect, there is no defect-induced level inside the energy gap near the Fermi-level. The change in the band gap is caused by the shift of the valence band maximum (VBM) and the conduction band minimum (CBM) in the band structure. In the case of oxygen vacancies (Fig. 3(b)), the CBM is shifted upward $\sim$0.15 eV, and the VBM moves down $\sim$0.05 eV. In the case of the hollow interstitial (Fig. 3(c)), the VBM shows no significant changes, however, the CBM moves upward $\sim$0.12 eV. In band structures with local tensile strain, the shift of the CBM has a primary influence on the change in the band gap and it is analogous to the changing trend of the band structure of GMO because of strain.[14] Briefly, the defect contributions to the

alternation of the band gap create the local tensile strain, as stated in the previous study.[14] However, as shown in Table 1, the band gap of structures with a local compressive strain near the defect decreases compared to that of the band gap of perfect GMO. To analyze the change in the band gap, it is necessary to investigate the band structure (Fig. 3(d) and (e)). The remarkable difference in the perfect band structure is the defect-induced flat band in the band gap. The structures with compressive strain have a dangling bond in common and this leads to the defect-induced level in the effective band structure. In the bridge interstitial, by the dangling bond of oxygen the defect-induced band crosses the Fermi level. The appearance of a band penetrating the Fermi level confirms metallic properties of the system of GMO with the bridge interstitial defect. In carbon vacancies, the overall band structure decreases and the CBM decreases even further. Additionally, it is considered that the unsaturated dangling bond generated by the carbon vacancy in GMO causes defect-induced states. The defect-induced level in the energy gap changes the band gap of structures with a local compressive strain near the defect.

4. Conclusion

The geometric and electronic structure of defective GMO was studied systematically using the density functional theory calculations. In terms of defect formation energy of each defective structure, oxygen vacancies and the interstitial oxygen on the bridge site were energetically more stable than the other two defects (carbon vacancies and the interstitial oxygen on the hollow site). The strain field induced by oxygen vacancies or the hollow interstitial oxygen results in local tensile strain near the defects, and the strain field of carbon vacancies and bridge interstitial results in local compressive strain. The band gaps of the defective GMO under local tensile stress are in good agreement with the previous study on the strain effect of GMO on band gap energy. However, interestingly, it was found that the change in the band gap energy of the other defects, such as carbon vacancies or interstitial oxygen on the bridge site, mainly resulted from the unsaturated dangling bond not from the strain effect. Moreover, it was found that a quite sensitive change in band gap energy (from metallic to semiconducting) could be engineered by the defect formation.

Acknowledgements

This research was supported by Basic Science Research Program through the National Research Foundation of Korea (NRF) funded by the Ministry of Education (2013R1A1A2A10064432).

References

1 K. S. Novoselov, A. K. Geim, S. V. Morozov, D. Jiang, Y. Zhang, S. V. Dubonos, I. V. Grigorieva and A. A. Firsov, Electric Field Effect in Atomically Thin Carbon Films, *Science*, 2004, **306**, 666–669.
2 D. Li and R. B. Kaner, Graphene-Based Materials, *Science*, 2008, **320**, 1170–1171.
3 A. K. Geim and K. S. Novoselov, The rise of graphene, *Nat. Mater.*, 2007, **6**, 183–191.
4 X. L. Li, X. R. Wang, L. Zhang, S. W. Lee and H. J. Dai, Chemically Derived, Ultrasmooth Graphene Nanoribbon Semiconductors, *Science*, 2008, **319**, 1229–1232.
5 Y. G. Semenov, K. W. Kim and J. M. Zavada, Spin field effect transistor with a graphene channel, *Appl. Phys. Lett.*, 2007, **91**, 153105.
6 Y. Zhang, T.-T. Tang, C. Girit, Z. Hao, M. C. Martin, A. Zettl, M. F. Crommie, Y. R. Shen and F. Wang, Direct observation of a widely tunable bandgap in bilayer graphene, *Nature*, 2009, **459**, 820–823.
7 S. B. Cho and Y.-C. Chung, Bandgap engineering of graphene by corrugation on lattice-mismatched MgO(111), *J. Mater. Chem. C*, 2013, **1**, 1595–1600.
8 Y. Qi, S. H. Rhim, G. F. Sun, M. Weinert and L. Li, Epitaxial Graphene on SiC(0001): More than Just Honeycombs, *Phys. Rev. Lett.*, 2010, **105**, 085502.
9 M. Y. Han, B. Ozyilmaz, Y. B. Zhang and P. Kim, Energy Band-Gap Engineering of Graphene Nanoribbons, *Phys. Rev. Lett.*, 2007, **98**, 206805.
10 X. R. Wang and H. J. Dai, Etching and narrowing of graphene from the edges, *Nat. Chem.*, 2010, **2**, 661–665.
11 L. A. Ponomarenko, F. Schedin, M. I. Katsnelson, R. Yang, E. W. Hill, K. S. Novoselov and A. K. Geim, Chaotic Dirac Billiard in Graphene Quantum Dots, *Science*, 2008, **320**, 356–358.
12 X. R. Wang, X. L. Li, L. Zhang, Y. Yoon, P. K. Weber, H. L. Wang, J. Guo and H. J. Dai, N-Doping of Graphene Through Electrothermal Reactions with Ammonia, *Science*, 2009, **324**, 768–771.
13 E. C. Mattson, H. H. Pu, S. M. Cui, M. A. Schoeld, S. Rhim, G. H. Lu, M. J. Nasse, R. S. Ruo, M. Weinert, M. Gajdardziska-Josifovska, J. H. Chen and C. J. Hirschmugl, Evidence of Nanocrystalline Semiconducting Graphene Monoxide during Thermal Reduction of Graphene Oxide in Vacuum, *ACS Nano*, 2011, **5**, 9710–9717.
14 H. H. Pu, S. H. Rhim, C. J. Hirschmugl, M. Gajdardziska-Josifovska, M. Weinert and J. H. Chen, Strain-induced bandgap engineering of graphene monoxide and its effect on graphene, *Phys. Rev. B: Condens. Matter Mater. Phys.*, 2013, **87**, 085417.
15 C. Kittel, *Introduction to solid state physics*, John Wiley & Sons, New York, 8th edn, 2005.
16 D. J. Appelhans, Z. Lin and M. T. Lusk, Two-dimensional carbon semiconductor: Density functional theory calculations, *Phys. Rev. B: Condens. Matter Mater. Phys.*, 2010, **82**, 073410.
17 J. Kotakoski, A. V. Krasheninnikov, U. Kaiser and J. C. Meyer, From Point Defects in Graphene to Two-Dimensional Amorphous Carbon, *Phys. Rev. Lett.*, 2011, **106**, 105505.
18 F. Banhart, J. Kotakoski and A. V. Krasheninnikov, Structural defects in graphene, *ACS Nano*, 2011, **5**, 26–41.
19 A. V. Krasheninnikov and F. Banhart, Engineering of nanostructured carbon materials with electron or ion beams, *Nat. Mater.*, 2007, **6**, 723–733.

20 F. Banhart, T. Fuller, P. Redlich and P. M. Ajayan, The formation, annealing and self-compression of carbon onions under electron irradiation, *Chem. Phys. Lett.*, 1997, **269**, 349–355.
21 K. Urita, K. Suenaga, T. Sugai, H. Shinohara and S. Iijima, In Situ Observation of Thermal Relaxation of Interstitial-Vacancy Pair Defects in a Graphite Gap, *Phys. Rev. Lett.*, 2005, **94**, 155502.
22 G. Kresse and J. Furthmuller, Efficient iterative schemes for ab initio total-energy calculations using a plane-wave basis set, *Phys. Rev. B: Condens. Matter Mater. Phys.*, 1996, **54**, 11169.
23 P. E. Blochl, Projector augmented-wave method, *Phys. Rev. B: Condens. Matter Mater. Phys.*, 1994, **50**, 17953.
24 J. P. Perdew, J. A. Chevary, S. H. Vosko, K. A. Jackson, M. R. Pederson, D. J. Singh and C. Fiolhais, Atoms, molecules, solids, and surfaces: Applications of the generalized gradient approximation for exchange and correlation, *Phys. Rev. B: Condens. Matter Mater. Phys.*, 1992, **46**, 6671.
25 J. P. Perdew and Y. Wang, Accurate and simple analytic representation of the electron-gas correlation energy, *Phys. Rev. B: Condens. Matter Mater. Phys.*, 1992, **45**, 13244.
26 J. Perdew, K. Burke and M. Ernzerhof, Generalized Gradient Approximation Made Simple, *Phys. Rev. Lett.*, 1996, **77**, 3865–3868.
27 H. Monkhorst and J. Pack, Special points for Brillouin-zone integrations, *Phys. Rev. B: Condens. Matter Mater. Phys.*, 1976, **13**, 5188–5192.
28 A. Ishii, M. Yamamoto, H. Asano and K. Fujiwara, DFT calculation for adatom adsorption on graphene sheet as a prototype of carbon nanotube functionalization, *J. Phys.: Conf. Ser.*, 2008, **100**, 052087.
29 W. H. Zhang, V. Carravetta, Z. Y. Li, Y. Luo and J. L. Yang, Oxidation states of graphene: Insights from computational spectroscopy, *J. Chem. Phys.*, 2009, **131**, 244505.
30 P. V. C. Medeiros, S. Stafstrom and J. Bjork, Effects of extrinsic and intrinsic perturbations on the electronic structure of graphene: Retaining an effective primitive cell band structure by band unfolding, *Phys. Rev. B: Condens. Matter Mater. Phys.*, 2014, **89**, 041407(R).
31 W. Ku, T. Berlijn and C.-C. Lee, Unfolding First-Principles Band Structures, *Phys. Rev. Lett.*, 2010, **104**, 216401.

